Organization and Representation of Boundary Layer Clouds

PETER BECHTOLD* AND PIER SIEBESMA

Royal Netherlands Meteorological Institute, De Bilt, the Netherlands

(Manuscript received 30 January 1997, in final form 5 August 1997)

ABSTRACT

This study is intended to summarize and to simplify the complicated processes in boundary layer cloud regimes using a single parameter, Q_1, the normalized saturation deficit.

With the aid of large eddy simulation (LES) data from different boundary layer cloud regimes it is illustrated i) that the in-cloud buoyancy flux is maximized when the fractional cloudiness approaches zero; ii) that the ensemble average buoyancy flux possesses two maxima, one for the trade wind cumulus case and one for the stratocumulus case; and iii) that the preferred mode for boundary layer clouds is either small cumuli or high values of cloudiness, and that cloudiness transitions from one regime to the other are difficult to represent numerically as in the transition regime the cloud-water-related variables are very parameter sensitive.

In addition, the importance of the contribution of the liquid water flux to the in-cloud and total buoyancy flux is outlined, and simple analytical and empirical methods are presented to compute the liquid water flux as a function of the fluxes of conserved variables for different boundary layer cloud regimes.

1. Introduction

We can go back as early as 1938 to the work of Bjerknes (the famous ''slice'' method) or later to the work of Asai and Kasahara (1967) to get a demonstration of the fact that boundary layer clouds, that is, shallow nonprecipitating convection, organize in such a way as to maximize the upward heat transport and that the buoyancy of cloudy updrafts in a clear environment is maximized as the fractional updraft area approaches zero. These results were confirmed by Randall (1987) using a classic convective mass flux model. One of the objectives of Randall was to bridge the gap between cumulus (Cu) convection as studied by the former authors and stratocumulus (Sc) convection. However, the shortcoming of the model applied by Randall is that there is no general method to determine the convective mass flux (this would require the knowledge of the fractional entrainment and detrainment rates) and the fractional area covered by updrafts.

The recent Atlantic Stratocumulus Transition Experiment (ASTEX) was dedicated to study the Sc to Cu transition over an oceanic region with strong surface temperature gradients. The observations revealed that the transformation of a Sc cloud field into a Cu cloud field implies an intermediate state with Cu occuring under the main Sc cloud deck (Bretherton et al. 1995a,b). However, it was difficult to develop a parameterization of cloudiness transitions from the observed data alone. Krueger et al. (1995a,b) studied the transformation of a Sc-topped boundary layer in a trade wind Cu type boundary layer using a 2D cloud ensemble model. One of their major findings was that the Sc to Cu transition can be explained by the observation that the differences between updraft and downdraft properties in the cloud layer gradually increase during the SCT; that is, the updrafts become more and more vigorous and the downdraft properties approach that of the environment. Furthermore, in contrast to a Sc boundary layer where the large eddy circulations extend over the entire boundary layer (cloud and subcloud layer), one observes separate cloud and subcloud layer circulations in the case of a Cu boundary layer, and only very few intense updrafts succeed in penetrating from the surface to the top of the cloud layer.

As shown by Betts (1973) or Hanson (1981), shallow nonprecipitating convection is essentially a mixing process. Therefore, a model that allows for nonlocal mixing should be able to represent the shallow convective boundary layer. Historically, essentially two types of models are utilized to represent boundary-layer clouds in mesoscale and large-scale numerical models, the mass flux model, and the turbulence ensemble model. We could enumerate here also the mixed-layer or bulk models, but this type of model contains elements of the first two types. Whereas mass flux models are generally used to describe the convective transport (which is propor-

* Current affiliation: Laboratoire d'Aérologie, Observatoire Midi-Pyrénées, Toulouse, France.

Corresponding author address: Dr. Peter Bechtold, Laboratoire d'Aérologie, Observatoire Midi-Pyrénées, 31400 Toulouse, France.
E-mail: becp@aero.obs-mip.fr

tional to the buoyancy flux) in Cu-topped boundary layers, turbulence ensemble models are generally used for Sc convection, where they proved to be very efficient (Bechtold et al. 1996). Bougeault (1981) was the first to apply a higher-order turbulence model to the trade wind boundary layer by relaxing the Gaussian cloud relations developed by Sommeria and Deardorff (1977) and Mellor (1977). Later, Lewellen and Yoh (1993) used binormal distributions to represent the fractional cloudiness in boundary layers with a non-Gaussian (positively skewed) structure, whereas Xu and Randall (1996) also tested the validity of simple analytical distribution functions for deep convective cases. Cuijpers and Bechtold (1995, hereafter referred to as CB) tried to generalize these statistical cloud relations by empirically determining the fractional cloudiness, the cloud water content, and the liquid water flux as a function of the normalized saturation deficit Q_1 using a large number of large eddy simulation (LES) data. Their results showed that apart from the trade wind Cu case the Gaussian cloud relations hold to a good approximation.

The objective of the present paper is to revisit the findings of CB using new LES data and to discuss the fundamental changes in the in-cloud buoyancy flux we observe as a function of the cloud fraction. It is not intended to derive a mathematical similarity between the mass flux and statistical model [the work of Wyngaard and Moeng (1992) can be considered as a first step in this direction]; however, the reader is guided in an intuitive way through the buoyancy flux concept that links the two models. Finally, even if not directly related, the recent approaches of Kain and Fritsch (1991) and Emanuel (1994), who tried to introduce some statistical mixing through a buoyancy sorting mechanism in a mass flux convection scheme, should also be seen in the context of the present problem.

2. Possible general buoyancy flux formulation

Using conserved thermodynamic variables, for convience we use here the liquid potential temperature $\theta_l = \theta(1 - Lq_l/c_pT)$ and the total water specific humidity $q_w = q_v + q_l$, the ensemble mean or grid-mean buoyancy flux can be written as

$$F_{\theta_v} = (1 + 0.61\overline{q}_w)F_{\theta_l} + \alpha F_{q_w} + \beta F_{ql}, \qquad (1)$$

where $\alpha = 0.61\overline{\theta}$ and $\beta = (\overline{\theta}/\overline{T})(L/c_p) - 1.61\overline{\theta}$. All notations are classic; that is, θ and T are the potential and absolute temperature respectively, q_l is the liquid water specific humidity, L is the specific heat of vaporization, and c_p is the specific heat of moist air at constant pressure.

In contrast to a mass flux model, the liquid water flux term in (1) cannot be determined directly in a turbulence model and must therefore be parameterized. Cuijpers and Bechtold showed that this term can be expressed as

$$F_{ql} = F_s N f_N, \qquad (2)$$

where N is the fractional cloudiness and f_N is a function that has the exact value of one in the special case that θ_l and q_w possess a joint Gaussian probability distribution—we come back to the particular function f_N later in this text. The variable s is defined as a linear combination of θ_l and q_w,

$$s = aq_w - b\theta_l + c, \qquad (3)$$

where the thermodynamic coefficients a, b, and c are derived utilizing a linearized form of the water vapor saturation relation (see appendix A). To fix the ideas, a is of order 10^{-1} and b of order 10^{-4}. Finally, using (2) we can rewrite the expression of the ensemble mean buoyancy flux (1) as

$$F_{\theta_v} = (1 + 0.61\overline{q}_w - \beta b f_N N)F_{\theta_l} + (\alpha + \beta a f_N N)F_{q_w}. \qquad (4)$$

This is our desired formulation, and we recognize that, apart from the ensemble average fluxes of θ_l and q_w that can be computed with any model, two further variable coefficients appear in (4), that is, the fractional cloudiness N and the flux enhancement factor f_N. As shown by CB these coefficients can be expressed as a function of the variable Q_1 only, where $Q_1 = c/\sigma_s$ is a normalized measure of the degree of saturation of the ensemble (e.g., for $Q_1 = 0$ the mean state is just saturated and the value of the fractional cloudiness is about 0.5).

The interesting point is that in addition to determining the factor f_N in (2) empirically as a function of Q_1 as done in CB, we can also compute f_N or the product $f_N N$ that intervenes in (4) directly from (2) using a mass flux approach. In a mass flux approach the flux of a variable Ψ is expressed as

$$F_\Psi = \overline{w'\Psi'} = \nu M_c(\Psi^u - \Psi^d), \qquad (5)$$

where M_c is the convective mass flux and ν is a proportionality factor. The superscripts u and d denote up- and downdraft values respectively. If we know the updraft and downdraft values of q_l, θ_l, and q_w, we can easily compute f_N from (2) using (5) and (3). In the limit of a trade wind Cu field the updraft values are equal to the cloudy values, that is, $\Psi^u = \Psi^c$, and the downdraft values are equal to the unsaturated environmental properties, $\Psi^d = \overline{\Psi}$. Furthermore, Bechtold and Cuijpers (1995) showed that the required cloudy values can be approximated by

$$q_l^c = \overline{q}_l/N; \qquad q_w^c = q_s(\overline{T}) + q_l^c;$$
$$\theta_l^c = \overline{\theta}(1 - Lq_l^c/c_p\overline{T}). \qquad (6)$$

The main assumption in (6) is that $\theta^c = \overline{\theta}$, but this approximation is generally good to within 0.2 K as shallow convective clouds tend to be slightly cooler than the environment. Therefore, in the trade wind Cu case we get from (2)–(3) and (5),

$$\nu M_c q_l^c = \nu M_c[a(q_w^c - \overline{q}_w) - b(\theta_l^c - \overline{\theta}_l)]Nf_N, \qquad (7)$$

and after some rearrangements using (6), we finally get

$$Nf_N = q_l^c/[a(q_s(\overline{T}) - \overline{q}_w) + q_l^c]. \quad (8)$$

In the other limit case of a Sc deck (i.e., $N \rightarrow 1$) (7) must be replaced by

$$\nu M_c(q_l^u - q_l^d) = \nu M_c[a(q_w^u - q_w^d) - b(\theta_l^u - \theta_l^d)]Nf_N. \quad (9)$$

If we now assume that the downdrafts are just saturated, then the updraft values are again given by (6) and the downdraft values by $q_l^d = 0$, $q_w^d = q_s(\overline{T})$, and $\theta_l^d = \overline{\theta}$. Using these values in (9) we finally obtain $Nf_N = 1$ so that f_N approaches the desired Gaussian limit value of one as $N \rightarrow 1$; note that the same result is obtained if it is assumed that the downdrafts contain some liquid water, for example, $q_l^d = 0.5q_l^u$.

3. Discussion

Large eddy simulation data for different meteorological situations have been generated including shallow GARP Atlantic Tropical Experiment (GATE) and deeper Barbados Oceanographic and Meteorological Experiment, (BOMEX) trade wind boundary layers with low (<20%) cloud cover, a cumulus-topped boundary layer observed over the North Sea (Smith and Jonas 1995), as well as boundary layers with intermediate cloud cover (ASTEX) and boundary layers topped by solid or broken Sc with cloud cover >80% (FIRE, SEMAPHORE).[1] With the aid of this data we can examine the dependence of the liquid water flux (2) and the buoyancy flux (4) as a function of the fractional cloudiness N or, more generally, as a function of the parameter Q_1. All simulations were run until a quasi steady state was reached. The horizontal and vertical resolutions were 125 and 50 m, respectively [see Siebesma and Cuijpers (1995) or CB for the technical details]. In addition to the data used in CB, we also use here data from a longtime (17 h) BOMEX run over a large computational domain as well as data from a 4-h North Sea cumulus run.

In this study the in-cloud values of the fluxes are of particular interest. Denoting the vertical velocity by w, the in-cloud value of the flux of a scalar field Ψ is defined as

$$F_\Psi = NF_\Psi^c + (1 - N)F_\Psi^e, \quad (10)$$

with

$$F_\Psi^c = (1/n)\sum_{i=1}^{n}(w_i - \overline{w})(\Psi_i - \overline{\Psi})$$

$$= (1/n)\left(\sum_{i=1}^{n} w_i\Psi_i - \overline{\Psi}\sum_{i=1}^{n} w_i\right), \quad (11)$$

where the subscript i stands for a cloudy sample, n denotes the total number of cloudy samples, and $\overline{w}$ is zero by definition. In the present study we evaluate (11) as well as the values of N and q_l at every vertical level in the cloud layer and try to represent all results as a function of a single parameter N or Q_1 only. We ignore any information about the structure of the cloud field as could be gained, for example, from the skewness parameter.

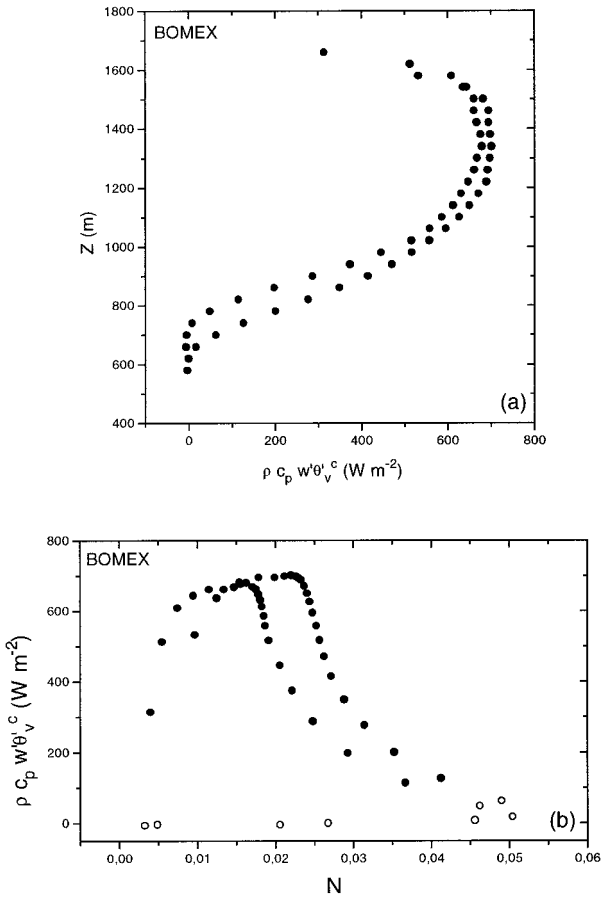

FIG. 1. The in-cloud buoyancy flux (W m^{-2}) as a function of height (a) and fractional cloudiness (b) from two 1-h time averages of a BOMEX simulation. In (b) the cloud base values are distinguished by open circles.

a. Trade wind Cu case

In Fig. 1a we have plotted the in-cloud buoyancy flux as defined in (10) as a function of height for the BOMEX case. The samples correspond to two 1-h averages taken after 10 and 17 h of simulation, respectively. The profiles produced by these two hourly averages are slightly shifted with respect to each other as cloud top and cloud base are slightly rising with time. We observe that close to the cloud base the in-cloud buoyancy flux is constant with height, then increases continously with height to very large values of up to 700 W m^{-2}, and finally de-

[1] FIRE: First ISCCP Regional Experiment SEMAPHORE: Structure des Echanges Mer-Atmosphère, Propriétés des Hétérogénéités Océaniques: Recherche Experimentale.

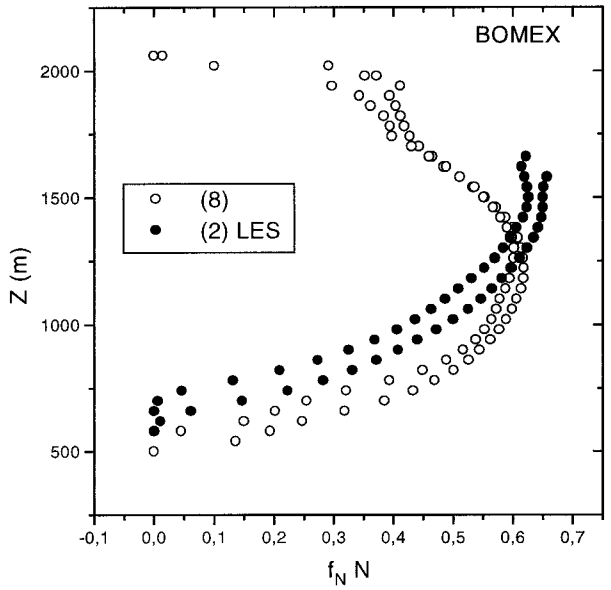

FIG. 2. The parameter $f_N N$ for BOMEX as computed from Eq. (2) (solid circles) and with the aid of the analytical solution (8) (open circles).

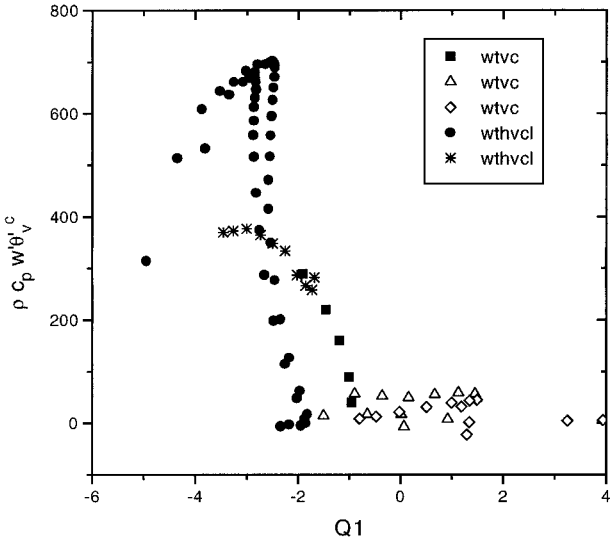

FIG. 3. The in-cloud buoyancy flux (W m^{-2}) for all experiments as a function of Q_1. The different experiments are denoted by different symbols. The FIRE and SEMAPHORE stratocumulus experiments are regrouped under the acronym FIRE.

creases again close to cloud top due to enhanced mixing with the environment.

In Fig. 1b we have replotted the same results as a function of the fractional cloudiness, but this time cloud base values are depicted separately by open circles. Again, we observe that the in-cloud buoyancy flux increases with decreasing cloudiness as the fractional cloudiness decreases with height. However, the cloud base values show a large scatter and do not fit on this monotonic function. As discussed in CB, the reason for this is that in trade wind Cu boundary layers the ensemble distribution in the active part of the cloud layer is different from the Gaussian distribution prevailing in the subcloud layer and for continuity reasons also at cloud base. Interestingly, also in three-dimensional high-resolution simulations of a single cumulus cloud [see, e.g., Fig. 6b in Vaillancourt et al. (1997)], one observes a Gaussian cloud base with relatively high cloud cover and a deep active part of the cloud with small cloud cover.

Finally, the BOMEX results are also utilized to compare the analytical approximation for the product $f_N N$ that intervenes in the buoyancy flux formulation with the actual values that are obtained from (2) computing the fluxes of q_l and s directly from the LES. In Fig. 2 the vertical profiles of $f_N N$ are illustrated using (2) and the analytical approximation (8). It turns out that the analytical solution (8) is an excellent approximation for both the shape of the profile and the absolute values of $f_N N$. The analytical solution (8) shows the expected parabolic profile we already observed in Fig. 1a; unfortunately, we could not use the experimental values using (2) for heights close to cloud top (above 1600 m) as the statistics become very bad (we are actually dividing two very small fluxes by each other). Furthermore, one should have in mind that the maximum values of about 0.6 for $f_N N$ compare favorably to the value of 0.03 that would be obtained using the Gaussian cloud relation $f_N N = N$.

b. All cloud types

Most of the transport in cloudy boundary layers is done by clouds. This means that the environment is more or less ''quiet'' and that the ensemble average buoyancy flux inside the cloud layer is to a good approximation given by the product of the in-cloud flux with the cloud fraction. The dependence of the in-cloud buoyancy flux as a function of Q_1 for all cloud types is illustrated in Fig. 3. Note that the Sc cases also include small values of the fractional cloudiness occuring at cloud base and cloud top levels. Figure 3 indicates that for each case the in-cloud buoyancy flux is a monotonic function of Q_1. In general, its magnitude increases from a value of order 10 W m^{-2} in the Sc case to a value of some hundreds W m^{-2} in the trade wind Cu case, with a particular strong increase in the interval $-3 < Q_1 < -1$. The in-cloud value of the buoyancy flux in the Sc case is of course close to the ensemble average value. Of course, it cannot be expected that for all cases the in-cloud flux is a universal function of one parameter only. However, we could not find any useful correlation between the in-cloud buoyancy flux and the skewness parameter.

Corresponding to Fig. 3, the flux enhancement factor f_N and the product $f_N N$ as computed from (2) are illustrated in Fig. 4. Similar to the in-cloud buoyancy

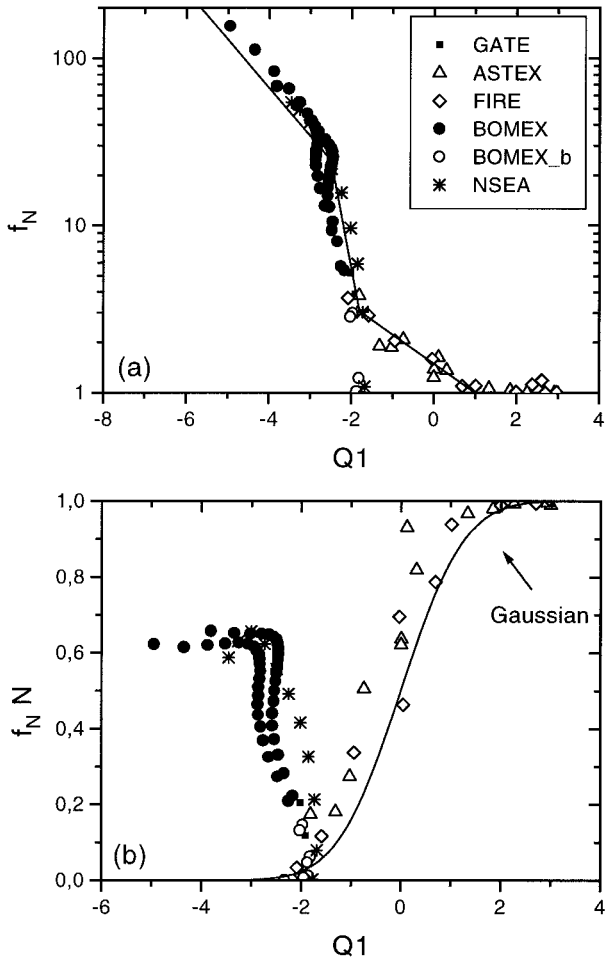

FIG. 4. As in Fig. 3 but for the coefficients f_N (a) and $f_N N$ (b). Additionally, cloud base values for the BOMEX case are denoted by open circles.

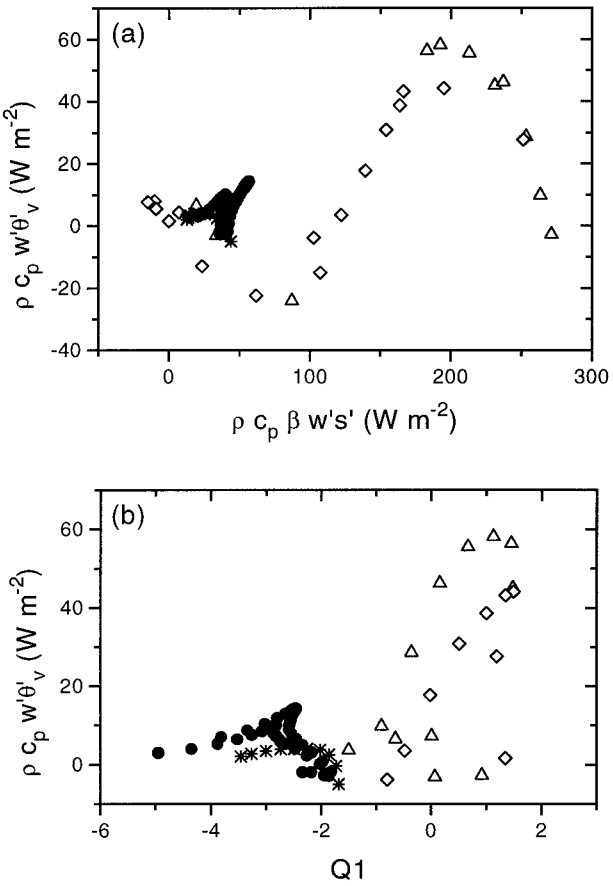

FIG. 5. As in Fig. 3 but for the ensemble average flux of θ_v as a function of the flux of s (a) and as a function of Q_1 (b).

flux, we observe a strong increase of the factor f_N (Fig. 4a) for $Q_1 < 0$. Its value increases exponentially from one in the Sc or Gaussian limit to infinity in the limit of $Q_1 \to -\infty$; that is, $N \to 0$. For completeness, we have approximated $f_N(Q_1)$ by a piecewise exponential function that is defined in appendix B. However, we stress that this functional dependence might not be universal and that the analytical solution (8) is preferable for practical applications. As seen from Fig. 4b, the product $f_N N$ shows a completely different behavior. We observe two maxima, one for the trade wind Cu case with a value of about 0.7 and the other for the Sc case with a value of 1. For the intermediate cloudiness cases with $-1.5 < Q_1 < 0$ corresponding to fractional cloudiness values ranging from about 15% to 50% the product $f_N N$ shows an absolute minimum. Here $f_N N$ is always limited to the theoretical interval [0, 1] as in the limit of $Q_1 \to -\infty$ the decrease in N is faster than the increase in f_N. For the Sc cases and the intermediate ASTEX Cu cases $f_N N$ is very well approximated by a Gaussian function (solid line in Fig. 4b) as $f_N = 1$ and, as shown in CB, N is approximately given by the Gaussian cloud relation $N = 0.5[1 + \text{erf}(Q_1/\sqrt{2})]$, where erf is the error function. However, the approximation of the factor f_N, as suggested in CB, was not sufficient as it does not assure the particular shape of the function $f_N N$ for $Q_1 < -1.5$. The possible parameterization of f_N and N is resumed in appendix B.

The above results for $f_N N$, that is, a double maximum for the trade wind Cu case and the Sc case and a minimum for intermediate cloudiness values, suggest that the ensemble average liquid water flux (2) and buoyancy flux (4) behave in a similar way. Indeed, it was suspected by Randall (1987) that the ensemble average buoyancy flux might attain its largest possible value for either a fully overcast or partly cloudy layer with $N \ll 1$. Similar to the previous plots, the ensemble average buoyancy flux is depicted in Fig. 5 as a function of the flux of s (a) and as a function of Q_1 (b). Figure 5b clearly resembles Fig. 4b and shows two maxima, one for the trade wind case with a maximum of roughly 20 W m^{-2} and one for the Sc case with maximum values of about 60 W m^{-2}. However, as expected, the scatter in Fig. 5 is much larger than in Fig. 4b, especially for the Sc and the intermediate cloudiness cases. In contrast to Fig. 5b,

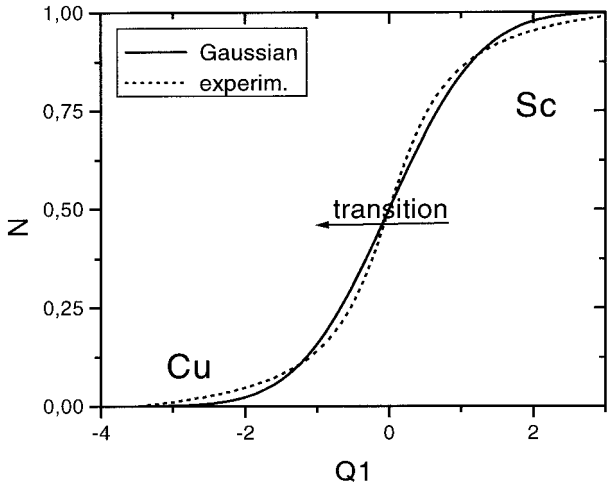

FIG. 6. The fractional cloudiness N as a function of Q_1. The dotted line denotes the experimental results of CB; the solid line is computed using the Gaussian assumption.

the scatter is greatly reduced in Fig. 5a, where we have replaced the dimensionless quantity Q_1 by the flux of *s*. Interestingly, we observe a pronounced maximum/minimum dependence for the Gaussian cases where the minimum for the Gaussian cases coincides with the flux maximum for the cumulus cases. However, these results must still be confirmed by a larger number of 3D long-time high-resolution simulations over large domains.

c. Theory and observations

Observations of boundary layer cloud cover (see, e.g., Henderson-Sellers and McGuffie 1991) show that the frequency of occurence of either small Cu or broken or solid Sc is high compared to the frequency of occurence of cloud fields with intermediate values of the cloud cover. When the observed cloud cover in octas is plotted against its frequency of occurence, one obtains a typical U-shaped probability function. The question is if this characteristic behavior is also intrinsically included in our present method of plotting the cloud-water-related variables as a function of Q_1.

In Fig. 6 we have replotted the fractional cloudiness N as a function of Q_1. The results are taken from CB who showed that N (not the factor f_N) can be well described by the Gaussian relation $N = 0.5[1 + \text{erf}(Q_1/\sqrt{2})]$. We recognize from Fig. 6 that for $Q_1 < -1$ small Cu clouds exists, whereas Sc can roughly be characterized by values of $Q_1 > 1$ measured in the bulk of the cloud layer. Therefore, the main changes in cloudiness from about 80% to 20% occur in the small interval $-1 < Q_1 < 1$. Furthermore, the maximum slope in the function $N(Q_1)$ occurs at $Q_1 = 0$, so that small changes in Q_1 (through turbulent mixing or radiative heating) imply that the cloud field with medium cloud cover evolves to the more ''stable'' regime of small Cu or Sc clouds. These findings are in accordance with that of Betts et al. (1995), who tried to parameterize cloudiness transitions as a function of the slope of the mixing line. Their conclusions were that the change in cloudiness with changing mixing line slope is so strong that it might be difficult from a modeling point of view to properly represent cloudiness transitions.

However, using dynamical arguments together with Figs. 4b and 5c we can even advance some further explanations concerning the characteristics of observed cloud distributions and cloudiness transitions. In Fig. 4b we observe two main branches, the Gaussian branch and the trade wind Cu branch. It appears that for each point on the Gaussian branch a positive perturbation of Q_1 (especially around $Q_1 = 0$) implies a larger buoyancy flux and so stronger mixing that might lead to even larger values of Q_1 and N, respectively. In contrast, when a positive Q_1 perturbation is applied to the trade wind Cu branch in Fig. 4b, the buoyancy flux strongly decreases (note the strong local minimum of the buoyancy flux at $Q_1 \approx -2$), which would mean less mixing so that the large negative values of Q_1 can persist. It follows that the trade wind Cu is a stable regime and might not evolve into a Gaussian high cloudiness Sc regime. Of course, this simple analysis cannot explain the complicated Sc to Cu transition as discussed by Bretherton and Wyant (1997) using decoupling arguments. But it is concordant with the fact the Sc is not directly transformed into a Cu cloud but the main Sc deck is eroded through increased cloud-top entrainment due to Cu clouds that form under and penetrate into the main Sc cloud deck.

4. Conclusions and perspectives

With the aid of LES data from different boundary layer cloud regimes we illustrated i) that the in-cloud buoyancy flux is maximized when the fractional cloudiness approaches zero; ii) that the ensemble average buoyancy flux possesses two maxima, one for the trade wind Cu case and one for the Sc case; and iii) that the preferred mode for boundary layer clouds are either small cumuli or high values of cloudiness, and that cloudiness transitions from one regime to the other are difficult to represent numerically as in the transition regime the cloud water related variables are very parameter sensitive. However, we further have to investigate the applicability of the above results to cases of active cumuli detraining below a strong inversion.

This study summarizes and generalizes the work of previous authors and shows that the ensemble average buoyancy flux can be represented as a function of the fluxes of conserved variables plus two additional variables: the fractional cloudiness and the flux enhancement factor f_N. It points out that the factor f_N, which is a measure for the deviation from the Gaussian distribution inside the boundary layer, is directly related to the in-cloud buoyancy flux. As the fractional cloudiness and the factor f_N are unique functions of the nor-

malized saturation deficit Q_1, it is in principle possible to represent in a consistent way cloudiness transitions as a function of the parameter Q_1. Alternatively to the empirical solution, an analytical solution for the product Nf_N based on a mass flux approach seems to be very attractive and accurate.

The authors hope that the present study on the organization of boundary layer clouds and their representation with the aid of a single parameter, Q_1, is a first step in the direction of developing unified cloud schemes, even if it would be desirable to have more data from longtime high-resolution LESs. The study conserves a general character as no assumptions about distributions were made and as it leaves open the question of how to compute the fluxes of conserved variables (either with a turbulence or a mass flux scheme). As an example, one line for future development could be the combination of a mass flux approach and a prognostic equation for the turbulent kinetic energy through Eq. (4). Finally, from a practical point of view the proposed boundary layer cloud representation depends on a reasonable estimation of the parameter Q_1; a discussion of this point is given in CB.

Acknowledgments. The first author is especially endebted to Prof. A. A. M. Holtslag for making his stay at KNMI a scientific and personal pleasure. We have also profited from discussions with Drs. J. W. M. Cuijpers, A. P. van Ulden, and A. C. Petersen. This work was supported by grants from program PATOM of CNRS/INSU (France). Computer facilities were made available by IDRIS (Paris, France).

APPENDIX A

Definition of Thermodynamic Coefficients

Let

$$a = (1 + L\overline{q}_{sl,T}/c_p)^{-1}, \qquad b = a(\overline{T}/\overline{\theta})q_{sl,T},$$
$$c = a(\overline{q}_w - \overline{q}_{sl}), \tag{A1}$$

where the temperature T_l and the saturation specific humidity q_{sl} are defined as $\overline{T}_l = \overline{\theta}_l(\overline{T}/\overline{\theta})$, $\overline{q}_{sl} = q_s(\overline{T}_l)$. Finally, $q_{sl,T}$ is defined as

$$\overline{q}_{sl,T} = \partial q_s/\partial T(T = \overline{T}_l) = Lq_s(\overline{T}_l)/(R_v\,\overline{T}_l^2), \tag{A2}$$

with R_v the gas constant of water vapor.

APPENDIX B

Parameterization of N, $\overline{q}_l$, and f_N

Following CB, the partial cloudiness and the ensemble average liquid water specific humidity can be parameterized as

$$N = \max\{0, \min[1, 0.5 + 0.36 \arctan(1.55Q_1)]\} \tag{B1}$$

$$\frac{\overline{q}_l}{\sigma_s} = \begin{cases} e^{-1} + 0.66Q_1 + 0.086Q_1^2, & Q_1 \geq 0 \\ e^{1.2Q_1 - 1}, & Q_1 < 0. \end{cases} \tag{B2}$$

Note that (B1) is a numerically simple and accurate approximation of the actual value of N, but due to the use of the arctan function we had to impose bounds to avoid erroneous values for large negative/positive values of Q_1.

The parameterization of the product $f_N N$ is more difficult. This can be done either by parameterizing directly the product $f_N N$ or by parameterizing each factor separately. As shown in Fig. 4b, for $Q_1 > -1.5$, $f_N N$ is well approximated by the Gaussian relation $f_N N = N$. For the remaining values of Q_1, $f_N N$ can be computed from the analytical approximation (8) after having computed N and $\overline{q}_l$ from (B1) and (B2). Another possibility consists in parameterizing f_N separately as a piecewise exponential function following Fig. 4a:

$$f_N = \begin{cases} 1, & Q_1 \geq 1 \\ e^{-0.4(Q_1 - 1)}, & -1.7 \leq Q_1 < 1 \\ 3 + e^{-3.8(Q_1 + 1.7)}, & -2.5 \leq Q_1 \leq -1.7 \\ 23.9 + e^{-1.6(Q_1 + 2.5)}, & Q_1 < -2.5. \end{cases}$$

REFERENCES

Asai, T., and A. Kasahara, 1967: A theoretical study of the compensating downward motions associated with cumulus clouds. *J. Atmos. Sci.,* **24,** 487–496.

Bechtold, P., and J. W. M. Cuijpers, 1995: Cloud perturbations of temperature and humidity: A LES study. *Bound.-Layer Meteor.,* **76,** 377–386.

——, S. K. Krueger, W. S. Lewellen, E. van Meijgaard, C.-H. Moeng, D. Randall, and A. van Ulden, 1996: Modeling a stratocumulus-topped PBL: Comparison between 1D models and with LES. *Bull. Amer., Meteor. Soc.,* **77,** 2033–2042.

Betts, A. K., 1973: Non-precipitating cumulus convection and its parameterization. *Quart. J. Roy. Meteor. Soc.,* **99,** 178–196.

——, C. S. Bretherton, and E. Klinker, 1995: Relation between mean boundary-layer structure and cloudiness at the R/V *Valdivia* during ASTEX. *J. Atmos. Sci.,* **52,** 2752–2762.

Bjerknes, J., 1938: Saturated-adiabatic ascent of air through dry-adiabatically descending environment. *Quart. J. Roy. Meteor. Soc.,* **64,** 325–330.

Bougeault, P., 1981: Modeling the trade-wind cumulus boundary layer. Part I: Testing the ensemble cloud relations against numerical data. *J. Atmos. Sci.,* **38,** 2414–2428.

Bretherton, C. S., and R. Pincus, 1995: Cloudiness and marine boundary layer dynamics in the ASTEX Lagrangian experiments. Part I: Synoptic setting and vertical structure. *J. Atmos. Sci.,* **52,** 2707–2723.

——, and M. C. Wyant, 1997: Moisture transport, lower-tropospheric stability, and decoupling of cloud-topped boundary layers. *J. Atmos. Sci.,* **54,** 148–167.

——, P. Austin, and S. T. Siems, 1995: Cloudiness and marine boundary layer dynamics in the ASTEX Lagrangian experiments. Part II: Cloudiness, drizzle, surface fluxes, and entrainment. *J. Atmos. Sci.,* **52,** 2724–2735.

Cuijpers, J. W. M., and P. Bechtold, 1995: A simple parameterization of cloud water related variables for use in boundary layer models. *J. Atmos. Sci.,* **52,** 2486–2490.

Emanuel, K. A., 1994: *Atmospheric Convection.* Oxford University Press, 580 pp.

Hanson, H. P., 1981: On mixing by trade-wind cumuli. *J. Atmos. Sci.*, **38,** 1003–1014.

Henderson-Sellers, A., and K. McGuffie, 1991: An investigation of the Burger distribution to characterize cloudiness. *J. Climate*, **4,** 1181–1209.

Kain, J. S., and J. M. Fritsch, 1990: A one-dimensional entraining/detraining plume model and its application in convective parameterization. *J. Atmos. Sci.*, **47,** 2784–2802.

Krueger, S. K., G. T. McLean, and Q. Fu, 1995a: Numerical simulation of the stratocumulus-to-cumulus transition in the subtropical marine boundary layer. Part I: Boundary-layer structure. *J. Atmos. Sci.*, **52,** 2839–2850.

——, ——, and ——, 1995b: Numerical simulation of the stratocumulus-to-cumulus transition in the subtropical marine boundary layer. Part II: Boundary-layer circulation. *J. Atmos. Sci.*, **52,** 2851–2868.

Lewellen, W. S., and S. Yoh, 1993: Binormal model of ensemble partial cloudiness. *J. Atmos. Sci.*, **50,** 1228–1237.

Mellor, G. L., 1977: The Gaussian cloud model relations. *J. Atmos. Sci.*, **34,** 356–358.

Randall, D. A., 1987: Turbulent fluxes of liquid water and buoyancy in partly cloudy layers. *J. Atmos. Sci.*, **44,** 850–858.

Siebesma, A. P., and J. W. M. Cuijpers, 1995: Evaluations of parametric assumptions for shallow cumulus convection. *J. Atmos. Sci.*, **52,** 650–666.

Smith, S. A., and P. Jonas, 1995: Observations of the turbulent fluxes in fields of cumulus clouds. *Quart. J. Roy. Meteor. Soc.*, **121,** 1185–1208.

Sommeria, G., and J. W. Deardorff, 1977: Subgrid-scale condensation in models of nonprecipitating clouds. *J. Atmos. Sci.*, **34,** 344–355.

Vaillancourt, P. A., M. K. Yau, and W. W. Grabowski, 1997: Upshear and downshear evolution of cloud structure and spectral properties. *J. Atmos. Sci.*, **54,** 1203–1217.

Wyngaard, J. C., and C.-H. Moeng, 1992: Parameterizing turbulent diffusion through the joint probability density. *Bound.-Layer Meteor.*, **60,** 1–13.

Xu, K.-M., and D. A. Randall, 1996: Explicit simulation of cumulus ensembles with the GATE phase III data: Comparison with observations. *J. Atmos. Sci.*, **53,** 3710–3736.